

## Subfemtosecond charge driving with correlation-assisted band engineering in a wide-gap semiconductor

Youngjae Kim and J. D. Lee\*

*Department of Emerging Materials Science, DGIST, Daegu 42988, Korea*

(Received 18 April 2018; revised manuscript received 6 November 2018; published 26 November 2018)

First-principles calculations indicate that, before falling into dielectric breakdown, charge transport induced by a strong-intensity few-cycle optical waveform in the subfemtosecond time domain can be precisely controlled depending on band distortion engineered by strain along the [0001] direction in wurtzite-AlN. It is further discovered from a model of electron-hole interaction that the subfemtosecond charge driving with band engineering can be substantially strengthened by excitonic correlation and dynamics. With these findings, we reveal band engineering to be a route to the ultrafast charge control of semiconductors and indeed suggest an unexplored prototype of solid-state petahertz ( $10^{15}$  Hz) device.

DOI: [10.1103/PhysRevB.98.195135](https://doi.org/10.1103/PhysRevB.98.195135)

### I. INTRODUCTION

Insight into the interaction between electron and high-intensity subfemtosecond laser pulse has opened a window on the extreme ultrafast dynamics at the time scale of 100 as ( $10^{-16}$  s)–1 fs ( $10^{-15}$  s) [1–10]. During the last decade, in particular, subfemtosecond electron dynamics instantaneously driven by few-cycle optical waveforms have attracted great attention to the potential of light-wave-induced solid-state electronics, which may dramatically increase the speed of the electric signal processing up to the petahertz ( $10^{15}$  Hz) frequency range. Realization of those light-wave-induced and -controlled dynamics have been attempted through not only charge [11–17] but also spin degrees of freedom [18].

It has been reported that macroscopic charge transport is generated by the light-wave-induced charge excitation in amorphous silica ( $\text{SiO}_2$ ), where the driven electric conductivity exceeds the static one by more than 18 orders [19]. This result represents a breakthrough in managing the electric current at a petahertz clock speed below the breakdown threshold, by manipulating a reversible wavelike flow of electrons. Theoretical investigations concerning such subcycle petahertz currents have been extensively carried out based on the independent-particle picture [20,21] or real-time first-principles dynamical simulation [22]. The real-time charge dynamics have been shown to depend on the crystal orientation, i.e., the localized current verges into delocalized tunneling along the bond axes of  $\text{SiO}_2$  [22]. Recently, the petahertz diode has been proposed to rectify the light-wave-induced current using a heterostructure made of low-hole-mass and low-electron-mass dielectrics [23], which implies that the oscillating current could actually be rendered and properly accessible for signal processing. More recently, the petahertz optical driving of carriers has also been demonstrated in a wide-gap semiconductor III-V nitride group (e.g., GaN) with efficient optical polarization, incorporating an interband

transition [24]. Broadening the material class from dielectrics to wide-gap semiconductors is important because semiconductors have (i) ubiquitous applications in modern electronics, (ii) efficient interband transition (a relatively weak-field optical pulse is available), (iii) good permittivity, (iv) diverse controls of electronic structure, and so on. Fine control of the material polarization now emerges as an important issue for realizing wide-range functionality of the solid-state petahertz device.

In this paper, we theoretically investigate light-wave-controlled subfemtosecond charge transport in a wide-gap III-V nitride semiconductor under a band distortion engineered by an external strain. In particular, wurtzite-AlN is known to have the largest piezoelectric coefficient of all III-V wurtzite materials [25] and its electronic structure is found to crucially change under a strain along the [0001] direction, which results in an increase in electron mobility and a subfemtosecond enhancement of charge transport. Further, that enhancement is found to be strongly intensified by the excitonic correlation according to a model investigation exploring the long-range electron-hole interaction. This demonstration shows band engineering to be a direction for subfemtosecond charge driving and control of semiconductors. In fact, it indicates the potential for the accurate processing of light-wave-controlled charge signals, by deploying band-engineered AlN plates.

The outline of the paper is as follows. In Sec. II, we investigate the subfemtosecond charge transport of AlN under an applied external strain within the framework of the time-dependent density functional theory (TDDFT). In Sec. III, we propose a one-dimensional two-band model incorporating the long-range excitonic correlation and study the light-wave-induced charge transport by solving the time-dependent Schrödinger equation. In the section, we also suggest a brief idea of the device application of the corresponding dynamics. Finally, in Sec. IV, we provide a summary and conclusion.

### II. BAND ENGINEERING

Comprehensive schematics of the light-wave-controlled charge dynamics in the wurtzite-AlN plate are displayed in

\*Corresponding author: [jdlee@dgist.ac.kr](mailto:jdlee@dgist.ac.kr)

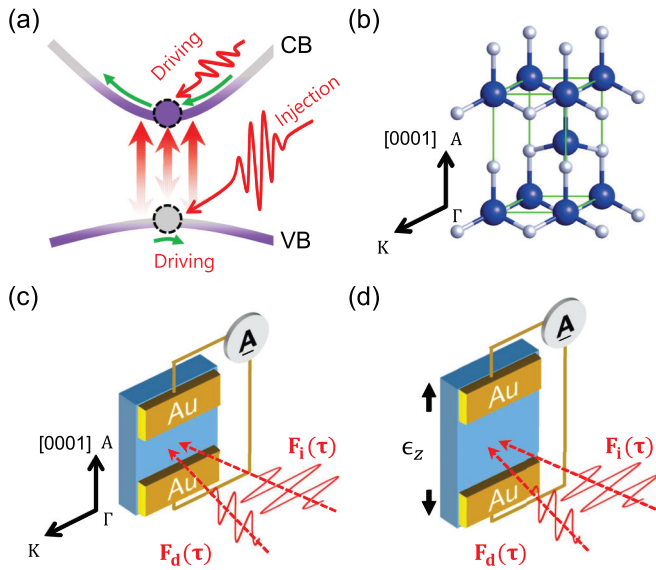


FIG. 1. (a) Schematics of carrier dynamics induced by two orthogonally polarized optical waveforms consisting of injection and driving pulses. (b) Crystal structure of wurtzite-AIN. Blue and white balls represent N and Al, respectively. (c),(d) A driving pulse along the  $\Gamma$ -A direction, together with an orthogonally polarized injection pulse, is applied to (c) the unstrained and (d) the strained AIN. An external tensile strain  $\epsilon_z$  is made along the [0001] direction, i.e.,  $\Gamma$ -A direction. Electrodes are positioned at both ends of the AIN system along the  $\Gamma$ -A direction. Only the current along the direction will then be measured by the Ampere meter.

Fig. 1. Figure 1(a) describes a situation in which a high-intensity pulse injects carriers into the conduction band (CB) from the valence band (VB) of AIN and another pulse drives an acceleration of carriers and induces the charge transport. The wurtzite-AIN crystal is depicted in Fig. 1(b). As shown in Figs. 1(c) and 1(d), the polarization direction of the injection pulse field  $\mathbf{F}_i(\tau)$  is tuned parallel to the  $\Gamma$ -K direction and that of the driving pulse field  $\mathbf{F}_d(\tau)$  to the  $\Gamma$ -A direction (i.e., the [0001] direction  $\propto \hat{z}$ ), which is the geometry in our consideration. The two pulses without time delay are orthogonal to each other in order to distinguish the dynamical processes between injection and driving. Those fields can be expressed from their vector potentials  $\mathbf{A}_i(\tau) = A_{i0} e^{-\tau^2/\tau_w^2} \sin(\omega\tau + \varphi) \hat{x}$  and  $\mathbf{A}_d(\tau) = A_{d0} e^{-\tau^2/\tau_w^2} \sin(\omega\tau + \varphi) \hat{z}$  as  $\mathbf{F}_i(\tau) = -\partial/\partial\tau \mathbf{A}_i(\tau)$  and  $\mathbf{F}_d(\tau) = -\partial/\partial\tau \mathbf{A}_d(\tau)$ , respectively, i.e., with  $F_{i0} = \omega A_{i0}$  and  $F_{d0} = \omega A_{d0}$ .  $\varphi$  is the carrier envelope phase (CEP), which is taken as  $\pi/2$  through the work unless mentioned otherwise because it gives the maximum charge transfer (shown later). Charge transport induced by the driving pulse is attained by  $Q_{tr} = \int_{-\infty}^{\infty} d\tau J(\tau)$ , where  $J(\tau)$  is the current density along the  $\Gamma$ -A direction [i.e., the current which will be probed by the Ampere meters in Figs. 1(c) and 1(d)].

In the calculation given later, the photon energy  $\omega$  of both pulses will be taken as 0.7 eV smaller than the band gap  $E_g$  of AIN ( $E_g = 4.19$  eV in our calculation [26]). The ponderomotive potential  $U_p (\equiv F_{i0}^2/4\omega^2)$  at the assumed value of  $F_{i0} = 0.7$  V/Å is then 1.9 eV, which is much larger than  $\omega$ . Also, the Keldysh parameter  $\gamma (\equiv \omega\sqrt{2E_g}/F_{i0})$  will be estimated to be  $\sim 1$ .  $U_p \gg \omega$  or  $\gamma \ll 1.5$  [27,28] would then

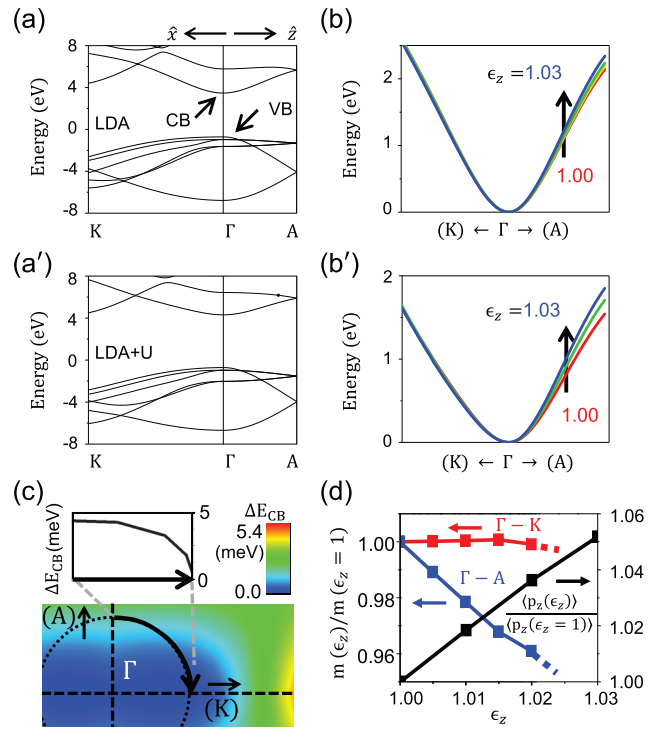


FIG. 2. (a) Electronic band structure of AIN. CB and VB represent the lowest conduction band and highest valence band, respectively. (b) Band distortions in CBs by the tensile strain  $\epsilon_z$ . (a'), (b') Electronic structure calculation with LDA+U. On-site Hubbard  $U$  for  $p$  orbitals of Al and N are adopted to be 5.44 and 1.36 eV, respectively. Electronic band structure and band distortions of CBs by the tensile strain  $\epsilon_z$  are given. A corrected gap is found to be 5.01 eV. (c) CB energy change  $\Delta E_{CB}$ , which is defined by  $E_{CB}(\epsilon_z = 1.03) - E_{CB}(\epsilon_z = 1)$  of (b), in the first Brillouin zone. The figure describes  $\Delta E_{CB}$  along the arc of the circle in the momentum space. Note that the bottoms of CBs at the  $\Gamma$  point are aligned with 0 eV in (b), (b'), and (c). (d) Relative effective mass and momentum ( $p_z$ ) expectation of CB near the  $\Gamma$  point (in fact, at a single grid point of  $\mathbf{k}$  mesh from the  $\Gamma$  point along the  $\Gamma$ -A direction) as a function of  $\epsilon_z$ .

be interpreted as a criterion of the adiabatic excitation and driving. In addition, the pulse width  $\tau_w$  is taken to be 3.66 fs, being short enough to avoid dielectric damage. To perform the theoretical exploration using the first-principles calculation, we employ TDDFT implemented in the full-potential linearized augmented plane wave (FP-LAPW) method within the ELK code [29].

Firstly, the static limit of AIN under a strain-engineered band distortion needs to be examined. Figure 2(a) shows the electronic structure of the unstrained AIN, which exhibits a direct band gap at the  $\Gamma$  point. When AIN is exposed to an external strain ( $\epsilon_z > 1$ ), a modulation occurs in CB along the  $\Gamma$ -A direction as displayed in Fig. 2(b) due to the strong piezoelectric coefficient, and concomitantly the band curvature increases along that direction. On the other hand, CB along the  $\Gamma$ -K direction is found to hardly change under the same strain. In Figs. 2(a') and 2(b'), LDA+U corrections in the band structure calculation are provided. In spite of the quantitative corrections, no serious qualitative renormalization is found. Through the work, therefore, LDA

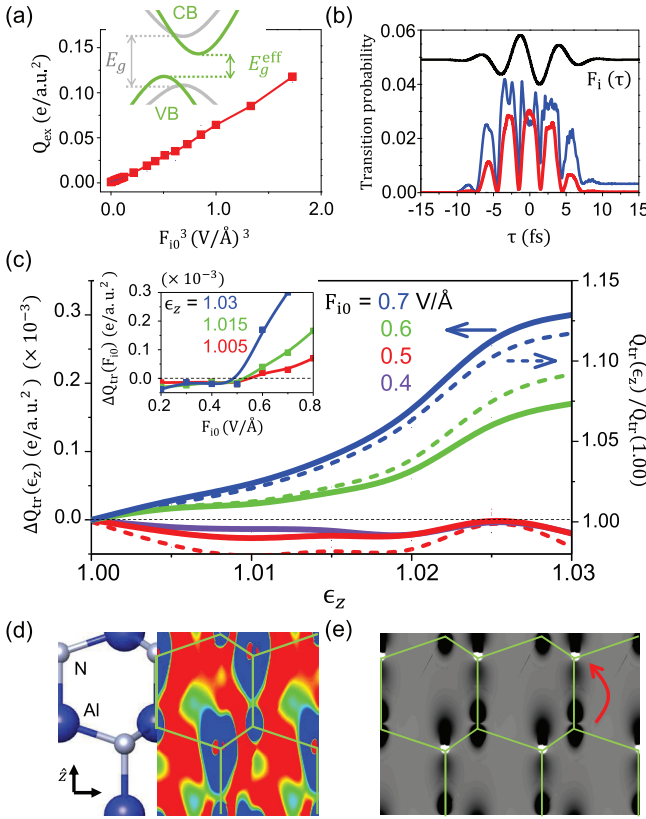


FIG. 3. (a) Excited charge  $Q_{\text{ex}}$  with respect to  $F_{10}^3$ . Inset shows the band structure in the ground state (gray) and the effective instantaneous band structure during the dynamics (green). Lateral and vertical shifts of conduction and valence bands are originated from  $\mathbf{p} - \mathbf{A}_d$  for electrons and  $\mathbf{p} + \mathbf{A}_d$  for holes, respectively. (b) Time-dependent transition probabilities. Red and blue lines are cases of  $F_{10} = 0.7 \text{ V/\AA}$  and  $1.5 \text{ V/\AA}$ , respectively. Black line denotes the electric field  $F_i(\tau)$  of the injection pulse. (c) Charge transfer  $\Delta Q_{\text{tr}}$  and its increment ratio  $[=Q_{\text{tr}}(\epsilon_z)/Q_{\text{tr}}(\epsilon_z = 1)]$  with respect to  $\epsilon_z$  at values of  $F_{10}$  and  $F_{d0} = 0.11 \text{ V/\AA}$ . Inset also gives the charge transport increment  $\Delta Q_{\text{tr}}$  with respect to  $F_{10}$  at values of  $\epsilon_z$  and  $F_{d0} = 0.11 \text{ V/\AA}$ . (d) Snapshot of the current density  $J(\tau)$  at  $\epsilon_z = 1.03$ . Red and blue domains correspond to positive and negative values of the current, respectively. (e) Difference in the electron density  $\Delta\rho$ , which is defined by  $\rho(\epsilon_z = 1.03) - \rho(\epsilon_z = 1)$ , after the optical pulse has passed. White and black clouds mean area with accumulated and dispersed charges, respectively.  $F_{10} = 0.7 \text{ V/\AA}$  and  $F_{d0} = 0.11 \text{ V/\AA}$  are taken in (d) and (e).

will be employed for the electronic structure calculation. In Fig. 2(c), the CB energy change  $\Delta E_{\text{CB}}$  caused by the strained distortion (at  $\epsilon_z = 1.03$ ) is plotted in the first Brillouin zone, where an increase in the band energy (i.e., the band curvature) along the  $\Gamma$ -A direction compared to other directions is obvious. This leads to a clear decrease in the CB effective mass along the  $\Gamma$ -A direction, but little change otherwise, and furthermore enhances the momentum expectation of  $\langle \text{CB} | p_z | \text{CB} \rangle$  near the  $\Gamma$  point [Fig. 2(d)].

Now the light-wave-controlled charge transports occurring on the subfemtosecond time domain are presented in Fig. 3. Excited charges  $Q_{\text{ex}}$  into CB by the injection pulse polarized along the  $\Gamma$ -K direction are found to follow roughly

$\propto F_{10}^3$  (in fact, roughly  $\propto F_{10}^3 F_{d0}^3$  [30]) in Fig. 3(a), which immediately signifies that the third-order process is engaged, i.e.,  $3\omega \approx E_g^{\text{eff}} \approx E_g - \langle \mathbf{A}_d(\tau) \cdot \mathbf{p} \rangle_{\text{CB}} - \langle \mathbf{A}_d(\tau) \cdot \mathbf{p} \rangle_{\text{VB}}$  with  $\langle \mathbf{A}_d(\tau) \cdot \mathbf{p} \rangle_{\text{CB}} \approx 1.44 \text{ eV}$  and  $\langle \mathbf{A}_d(\tau) \cdot \mathbf{p} \rangle_{\text{VB}} \approx 0.6 \text{ eV}$  in the calculation. In the inset,  $E_g^{\text{eff}}$  is an effective energy gap reduced due to the intraband transition and intense laser field (indicating a temporal modulation of the light-matter interacting band structures) [31], at which the charge excitation would be made most actively. In Fig. 3(b), the carrier excitation by the injection field can be reached through the real-time transition probability  $|\langle \text{CB} | \text{VB}(\tau) \rangle|^2$ .  $|\text{VB}(\tau)\rangle$  corresponds to the time-evolved wave function of valence electron state, which can be managed within the framework of TDDFT. A field strength  $F_{\text{fail}}$  giving rise to the dielectric breakdown is empirically estimated to be  $F_{\text{fail}} \gtrsim E_g/a$  [16] so that it gives about  $1.35 \text{ V/\AA}$  for AlN with a lattice constant  $a \approx 3.1 \text{ \AA}$ . Here it is interesting to compare the real-time probabilities between  $0.7 \text{ V/\AA}$  and  $1.5 \text{ V/\AA}$ . At  $0.7 \text{ V/\AA}$ , a signal profile turns out to be completely reversible at the petahertz control rate, while at  $1.5 \text{ V/\AA}$ , the profile is no longer reversible even after a complete pass of the injection pulse, which is a clear symptom of dielectric breakdown. Charge transports at  $F_{d0} = 0.11 \text{ V/\AA}$  are provided as their increments  $\Delta Q_{\text{tr}} [=Q_{\text{tr}}(\epsilon_z) - Q_{\text{tr}}(\epsilon_z = 1)]$  and increment ratios  $Q_{\text{tr}}(\epsilon_z)/Q_{\text{tr}}(\epsilon_z = 1)$  in Fig. 3(c). It is explicitly shown that  $Q_{\text{tr}}$  gradually increases in terms of the band engineering according to the enhancement in charge mobility, consistent with Fig. 2. In that sense, we note that  $Q_{\text{tr}}$  can be made to increase a lot in a controlled fashion. Intriguingly, the inset in Fig. 3(c) reveals the existence of a critical field strength  $F_c$  to give a threshold initiating an appreciable  $\Delta Q_{\text{tr}}$ .  $F_c$  can be estimated from  $3F_c d_{\Gamma-K} \approx E_g^{\text{eff}}$ , where the third-order process is considered [Fig. 3(a)] on the basis of the static electronic structure and  $d_{\Gamma-K}$  ( $\approx 1.89 \text{ \AA}$ ) is the interatomic bond length of Al-N along the  $\Gamma$ -K direction. This gives  $F_c \approx 0.4 \text{ V/\AA}$ , a value consistent with the inset in Fig. 3(c). Figure 3(d) represents a snapshot of the current density of injected charges in the real space. Injected charges appear to form an optical-field-driven conducting channel through the Al-N bond along the  $\Gamma$ -A direction, such that those charges flow through the channel. Of course, the channel is also activated by the strain. This is confirmed in Fig. 3(e), which shows a difference in the charge density  $\Delta\rho$  between  $\epsilon_z = 1.03$  and  $\epsilon_z = 1$  after the optical pulse has completely passed. Charge transfers from Al to N are obvious in the figure.

### III. EXCITONIC CORRELATION

To capture the complete dynamical nature beyond TDDFT, we address a model Hamiltonian  $\mathcal{H}$  to contain the electron-hole interaction based on the one-dimensional (along the driving pulse polarization, i.e., the  $\Gamma$ -A direction) tight-binding approximation [23]. The Hamiltonian  $\mathcal{H}$  reads as follows:

$$\begin{aligned} \mathcal{H} = & \sum_k E_k^e(\tau) c_k^\dagger c_k + \sum_{k'} E_{k'}^h(\tau) d_{k'}^\dagger d_{k'} \\ & + \sum_{kk'} \sum_q v(q) c_k^\dagger c_{k-q} d_{k'}^\dagger d_{k'+q} \\ & + \bar{p} [A_d(\tau) + A_i(\tau)] \sum_k (c_k^\dagger d_{-k}^\dagger + d_{-k} c_k). \end{aligned} \quad (1)$$

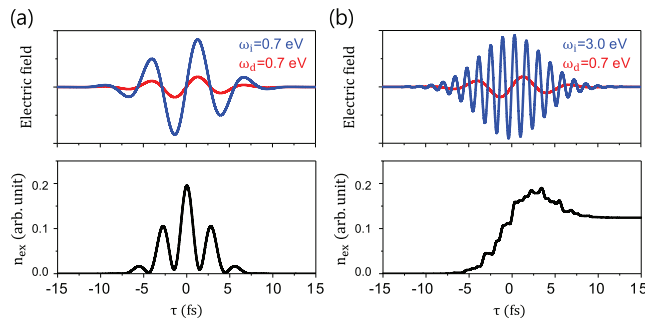


FIG. 4. (a) Adiabatic response of carriers. (b) As  $\omega_i$  approaches the resonance, the response becomes nonadiabatic. Note that  $n_{\text{ex}}(\tau)$ , i.e., the number of excited electron-hole pairs, is given by  $\sum_{kk'} |G(k, k', \tau)|^2$ .  $F_{i0} = 0.7$  V/Å,  $F_{d0} = 0.15$  V/Å, and  $V_0 = 1.0$  eV are used.

The first term in  $\mathcal{H}$  represents the effective band energies of electrons and holes of a given semiconductor, that is,  $E_k^e(\tau)$  and  $E_k^h(\tau)$  are given by  $E_k^e(\tau) = \varepsilon_k^e - p_d^e A_d(\tau) \sin(ka)$  and  $E_k^h(\tau) = \varepsilon_k^h + p_d^h A_d(\tau) \sin(ka)$  for electrons and holes, respectively.  $a$  is the lattice constant.  $\varepsilon_k^e$  and  $\varepsilon_k^h$  are the tight-binding band energies at the wave vector  $k$ , i.e.,  $\varepsilon_k^e = E_g/2 + \Delta^e [1 - \cos(ka)]$  and  $\varepsilon_k^h = E_g/2 + \Delta^h [1 - \cos(ka)]$ . The time dependence of effective band energies comes from combining the intraband transition due to  $\mathbf{A}_d(\tau)$ . In fact,  $p_d^e$  and  $p_d^h$  are the matrix elements governing the intraband transition. Within the tight-binding picture, electron hopping is obtained from its kinetic energy like  $\Delta^e/4 = \langle l | (p_e^2/2) | l + 1 \rangle = \langle l | p_e | l \rangle \langle l | p_e | l + 1 \rangle = \bar{p} p_d^e$ , where  $l$  denotes the site index and  $\bar{p}$  and  $p_d^e$  correspond to  $\langle l | p_e | l \rangle$  and  $\langle l | p_e | l + 1 \rangle$ , respectively. We then have the effective electron band energy,  $E_k^e(\tau) = \varepsilon_k^e - [\Delta^e A_d(\tau)/4\bar{p}] \sin(ka)$  and also the effective hole band energy in the same fashion.  $\langle l | p_e | l \rangle = \langle l | p_h | l \rangle = \bar{p}$  is assumed. The second term in  $\mathcal{H}$  gives the attractive potential between electron and hole to bring about the excitonic correlation. This may be approximated as a long-wavelength sector of the (screened) Coulomb interaction like  $v(q) = -(2\pi/L)(1/2q_c)V_0\Theta(q_c - |q|)$  [32–35].  $\Theta(q)$  is the Heaviside step function. The last term in  $\mathcal{H}$  describes the interband transition between CB and VB. For an actual calculation, the parameters of  $E_g = 4.5$  eV,  $\Delta^e = 4.5$  eV,  $\Delta^h = 2.0$  eV, and  $\bar{p}/\omega = 3$  Å are taken and the cutoff wave vector  $q_c = \pi/20a$  is set.

Dynamics under the double-pulse optical pumping can be described by solving the time-dependent Schrödinger equation  $i\partial/\partial\tau|\Psi(\tau)\rangle = \mathcal{H}|\Psi(\tau)\rangle$ .  $|\Psi(\tau)\rangle$  is the quantum mechanical state of the total system, which can be written as  $|\Psi(\tau)\rangle = G(\tau)|0, 0\rangle + \sum_{k,k'} G(k, k', \tau)|k, k'\rangle$ .  $|0, 0\rangle$  means the vacuum state of  $|0\rangle_c|0\rangle_v$  and  $|k, k'\rangle$  now indicates  $c_k^\dagger d_{k'}^\dagger |0\rangle_c |0\rangle_v$ . The time-dependent Schrödinger equation leads to a population imbalance around the  $\Gamma$  point and makes the light-wave-induced current  $J(\tau) = \sum_{kk'} [p_d^e \sin(ka) + p_d^h \sin(k'a)] |G(k, -k', \tau)|^2$  [23].

It is important to realize the adiabatic dynamics of carriers accompanying the excitonic Coulomb interaction at the petahertz clock speed. Figure 4(a) displays that the dynamics at  $V_0 = 1.0$  eV are shown to be adiabatic in that  $n_{\text{ex}}(\tau)$  simply

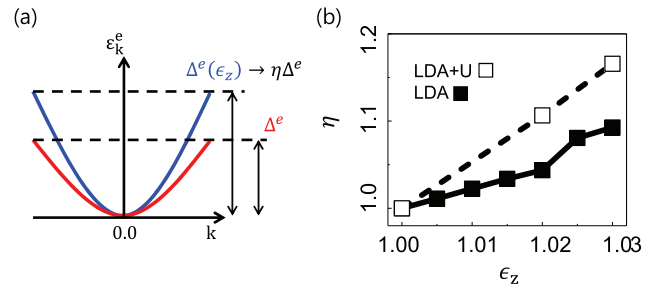


FIG. 5. (a) Relation between the band width modification parameter  $\eta$  and the crystal strain  $\varepsilon_z$ . (b)  $\eta$  is determined by an estimation of the conduction band width ( $\eta\Delta^e$ ) as a function of the strain  $\varepsilon_z$  from LDA and LDA+U [see Figs. 2(b) and 2(b')].

follows the field oscillation of the optical pulse under the condition of  $E_g \gg \omega_i = \omega_d = \omega$ .  $\omega_i$  and  $\omega_d$  are frequencies of the injection and driving pulses, respectively. In the condition, the carrier generation and driving become mutually synchronous. In contrast, in Fig. 4(b), as  $\omega_i$  approaches the resonance, the adiabaticity is found to fail. Carriers would then be nonadiabatically excited and remain even after the injection pulse has passed. It may be worth noting that the experimental setup corresponding to Fig. 4(b) can be used for the high-order sideband generation in semiconductors [36].

To simulate the strain effect, we attempt to control the conduction band width by putting  $\Delta^e \rightarrow \eta\Delta^e$ , where  $\eta$  plays a role of the band width modification parameter. In Fig. 5, it is shown that the strain  $\varepsilon_z$  from 1.0 to 1.03 quantitatively corresponds to the band modification of  $\eta\Delta^e$  with  $\eta$  from 1.0 to 1.1 (or from 1.0 to 1.16) according to the first-principles calculation of LDA (or LDA+U). Consequently, in the following model calculation, we focus on a range of  $\eta$  up to 1.2.

Schematic of the effective electron (CB) and hole (VB) bands at a given time  $\tau$  according to the effective Hamiltonian  $\mathcal{H}$  is illustrated in Fig. 6(a). Figure 6(b) shows the charge transfer  $Q_{\text{tr}}$  with respect to  $\varphi$ , i.e., CEP, where the maximal transfer occurs at  $\varphi = \pi/2$ . Charge transports are enhanced by the band width modification parameter  $\eta$  and the injection pulse strength  $F_{i0}$  [Fig. 6(c)]. The band modification of  $\eta\Delta^e$  with  $\eta \approx 1.1$  in the model calculation quantitatively corresponds to the strain-induced change (at the 3% strain, i.e.,  $\varepsilon_z \approx 1.03$ ) in the first-principles band structure of LDA results of Fig. 5 [also see Fig. 2(b)]. Compared to Fig. 3(c), a critical scale such as  $F_c$  is not observed because the material dimension along the injection pulse polarization (i.e.,  $\Gamma$ -K direction) is completely suppressed in the present model, which is different from the TDDFT calculation of AlN. Interestingly, nevertheless, charge transports such as in Fig. 6(c) are found to be further enhanced by turning on the excitonic correlation  $v(q)$ . For instance, they are strengthened by about three times more at  $V_0 = 1$  eV than 0 eV as shown in Fig. 6(d). It is understood from Fig. 6(e) that by the excitonic correlation, scattered momenta of excited carriers may suppress stimulated recombination during the dynamics and consequently, more pairs of excited electrons and holes are sustained, which could then participate in the resultant charge transfers. Recently, it was actually pointed out that the excited carrier occupation during the attosecond carrier injection into GaAs increases

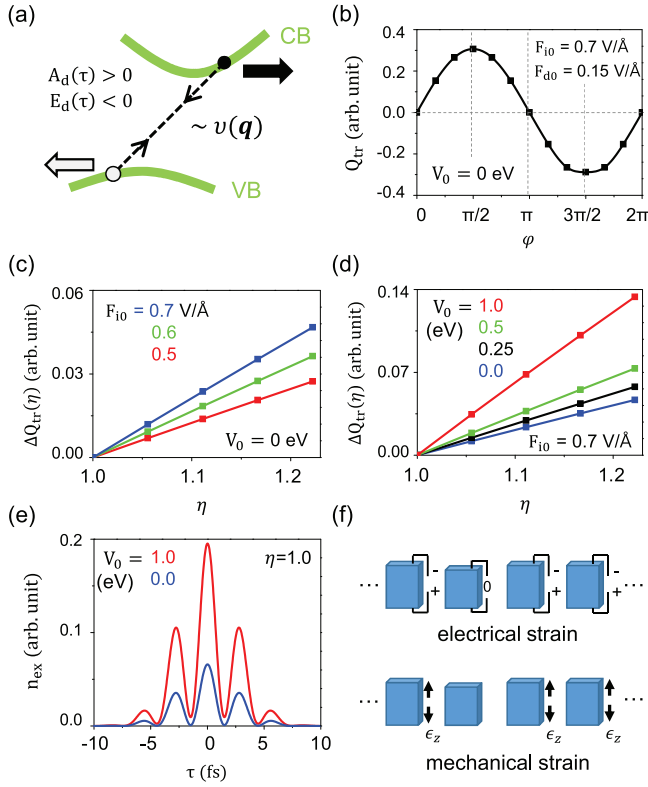


FIG. 6. (a) Schematic of effective bands  $E_k^c(\tau)$  (CB) and  $E_k^h(\tau)$  (VB) at a given time  $\tau$ . Block arrows at electron (CB) and hole (VB) denote each propagation direction at the time. (b) Charge transport  $Q_{tr}$  with respect to  $\phi$ , i.e., CEP. (c) Charge transport increment  $\Delta Q_{tr}$  as a function of the band width modification parameter  $\eta$  at values of  $F_{10}$ . (d) Charge transport with the excitonic-correlation-assisted band engineering.  $\Delta Q_{tr}$  as a function of the parameter  $\eta$  at values of  $V_0 = 1.0, 0.5, 0.25,$  and  $0$  eV.  $F_{d0} = 0.15$  V/Å is adopted in (c) and (d). (e) The number of excited electron-hole pairs,  $n_{ex}(\tau)$ .  $F_{10} = 0.7$  V/Å and  $F_{d0} = 0.15$  V/Å are used. (f) (upper panel) Strain may be applied in an electrical way such that the signal array of ...1011... would be removable or rewritable. (lower panel) Strain may be applied in a mechanical way such that the signal array of ...1011... would be less removable or less rewritable.

significantly due to intraband motion [37]. Considering this, the Coulomb scattering would be a source of the intraband transition (i.e.,  $c_k^\dagger c_{k-q}$  for electrons and  $d_k^\dagger d_{k'+q}$  for holes) and result in a coherent increase of carriers. It will then be a general expectation that the long-range excitonic correlation

should support the optically induced charge dynamics of semiconductors.

Application of the strain could be done in two ways. One is an electrical way, where the compressive or tensile strain is generated by an applied voltage to the AlN plate due to an electromechanical interaction, i.e., the piezoelectric effect. The other is a mechanical way, where mechanical tension may be produced in the AlN plate by a suitable substrate. Manipulating the band structure of the AlN plate in either way, the signal array of... 1011... could be prepared in terms of strained or unstrained AlN plates as shown in Fig. 6(f). Subfemtosecond readouts of the arrayed signals have been discussed throughout the work, being enabled in the double-pulse geometry in Fig. 1. Depending on whether the strain is applied electrically or mechanically, the signal processing could be obtained in a volatile manner or in a (almost) non-volatile manner [Fig. 6(f)]. In particular, although the volatile operation including the petahertz application of strain (i.e., petahertz writing) may have difficulties at the current stage, the nonvolatile operation of only the petahertz reading from the permanently applied strain to AlN would have practicalities. This would be an example where the light-wave-induced current could be directly accessible for petahertz electronic signal processing in memory devices.

#### IV. SUMMARY AND CONCLUSION

To summarize, we have theoretically investigated light-wave-controlled charge transport through the band engineering of a wide-gap semiconductor AlN with real-time subfemtosecond dynamics of optical injection and driving of carriers by high-intensity subcycle optical waveforms. Subfemtosecond charge transport was found to be enhanced by the external tensile strain along the [0001] direction of AlN within the framework of the first-principles TDDFT. In addition, their strong excitonic reinforcements were addressed by scrutinizing their dynamical nature beyond TDDFT, using a model of electron-hole interaction in strained semiconductors. This demonstration proposes that wide-gap wurtzite semiconductors could be used for base materials for a solid-state petahertz device with diverse ramifications, which eventually concludes that the band engineering can be a guidance to the subfemtosecond physics of semiconductors.

#### ACKNOWLEDGMENT

This work was supported by the Basic Science Research Program (2016R1A2B4013141) through the National Research Foundation of Korea (NRF) funded by the Ministry of Science and ICT.

[1] F. Krausz and M. Ivanov, *Rev. Mod. Phys.* **81**, 163 (2009).  
 [2] T. Brabec and F. Krausz, *Rev. Mod. Phys.* **72**, 545 (2000).  
 [3] M. Uiberacker, Th. Uphues, M. Schultze, A. J. Verhoeft, V. Yakovlev, M. F. Kling, J. Rauschenberger, N. M. Kabachnik, H. Schröder, M. Lezius, K. L. Kompa, H.-G. Müller, M. J. J. Vrakking, S. Hendel, U. Kleineberg, U. Heinzmann, M. Drescher, and F. Krausz, *Nature (London)* **446**, 627 (2007).

[4] M. Schultze, M. Fieß, N. Karpowicz, J. Gagnon, M. Korbman, M. Hofstetter, S. Neppl, A. L. Cavalieri, Y. Komninos, Th. Mercouris, C. A. Nicolaides, R. Pazourek, S. Nagele, J. Feist, J. Burgdörfer, A. M. Azzeer, R. Ernstorfer, R. Kienberger, U. Kleineberg, E. Goulielmakis, F. Krausz, and V. S. Yakovlev, *Science* **328**, 1658 (2010).  
 [5] F. Krausz and M. I. Stockman, *Nat. Photonics* **8**, 205 (2014).

- [6] J. D. Lee, *Phys. Rev. Lett.* **111**, 027401 (2013).
- [7] K. T. Kim, C. Zhang, A. D. Shiner, B. E. Schmidt, F. Legare, D. M. Villeneuve, and P. B. Corkum, *Nat. Photonics* **7**, 958 (2013).
- [8] K. Klünder, J. M. Dahlström, M. Gisselbrecht, T. Fordell, M. Swoboda, D. Guénot, P. Johnsson, J. Caillat, J. Mauritsson, A. Maquet, R. Taïeb, and A. L'Huillier, *Phys. Rev. Lett.* **106**, 143002 (2011).
- [9] S. Ghimire, A. D. DiChiara, E. Sistrunk, P. Agostini, L. F. DiMauro, and D. A. Reis, *Nat. Phys.* **7**, 138 (2011).
- [10] O. Schubert, M. Hohenleutner, F. Langer, B. Urbanek, C. Lange, U. Huttner, D. Golde, T. Meier, M. Kira, S. W. Koch, and R. Huber, *Nat. Photonics* **8**, 119 (2014).
- [11] R. Kienberger, E. Goulielmakis, M. Uiberacker, A. Baltuska, V. Yakovlev, F. Bammer, A. Scrinzi, Th. Westerwalbesloh, U. Kleineberg, U. Heinzmann, M. Drescher, and F. Krausz, *Nature (London)* **427**, 817 (2004).
- [12] M. Schultze, E. M. Bothschafter, A. Sommer, S. Holzner, W. Schweinberger, M. Fiess, M. Hofstetter, R. Kienberger, V. Apalkov, V. S. Yakovlev, M. I. Stockman, and F. Krausz, *Nature (London)* **493**, 75 (2013).
- [13] E. Goulielmakis, Z.-H. Loh, A. Wirth, R. Santra, N. Rohringer, V. S. Yakovlev, S. Zherebtsov, T. Pfeifer, A. M. Azzeer, M. F. Kling, S. R. Leone, and F. Krausz, *Nature (London)* **466**, 739 (2010).
- [14] A. L. Cavalieri, N. Müller, Th. Uphues, V. S. Yakovlev, A. Baltuška, B. Horvath, B. Schmidt, L. Blümel, R. Holzwarth, S. Hendel, M. Drescher, U. Kleineberg, P. M. Echenique, R. Kienberger, F. Krausz, and U. Heinzmann, *Nature (London)* **449**, 1029 (2007).
- [15] C. Lemell, S. Neppl, G. Wachter, K. Tökési, R. Ernstorfer, P. Feulner, R. Kienberger, and J. Burgdörfer, *Phys. Rev. B* **91**, 241101(R) (2015).
- [16] O. Kwon, T. P.-Colberg, V. Apalkov, B. K. Kim, J. J. Kim, M. I. Stockman, and D. Kim, *Sci. Rep.* **6**, 21272 (2016).
- [17] O. Kwon and D. Kim, *Appl. Phys. Lett.* **108**, 191112 (2016).
- [18] Y. Kim and J. D. Lee, *Phys. Rev. B* **97**, 041105(R) (2018).
- [19] A. Schiffrin, T. P.-Colberg, N. Karpowicz, V. Apalkov, D. Gerster, S. Mühlbrandt, M. Korbman, J. Reichert, M. Schultze, S. Holzner, J. V. Barth, R. Kienberger, R. Ernstorfer, V. S. Yakovlev, M. I. Stockman, and F. Krausz, *Nature (London)* **493**, 70 (2013).
- [20] S. Y. Kruchinin, M. Korbman, and V. S. Yakovlev, *Phys. Rev. B* **87**, 115201 (2013).
- [21] P. G. Hawkins and M. Y. Ivanov, *Phys. Rev. A* **87**, 063842 (2013).
- [22] G. Wachter, C. Lemell, J. Burgdörfer, S. A. Sato, X.-M. Tong, and K. Yabana, *Phys. Rev. Lett.* **113**, 087401 (2014).
- [23] J. D. Lee, W. S. Yun, and N. Park, *Phys. Rev. Lett.* **116**, 057401 (2016).
- [24] H. Mashiko, K. Oguri, T. Yamaguchi, A. Suda, and H. Gotoh, *Nat. Phys.* **12**, 741 (2016).
- [25] F. Bernardini, V. Fiorentini, and D. Vanderbilt, *Phys. Rev. B* **56**, R10024(R) (1997).
- [26] An experimental energy gap of AlN is observed about 6.2 eV in I. Vurgaftman and J. R. Meyer, *J. Appl. Phys.* **94**, 3675 (2003).
- [27] C. B. Schaffer, A. Brodeur, and E. Mazur, *Meas. Sci. Technol.* **12**, 1784 (2001).
- [28] H. R. Reiss, *Phys. Rev. A* **75**, 031404(R) (2007).
- [29] In the TDDFT calculation, the local density approximation (LDA) of Ceperley-Alder exchange correlation functional based on Perdew-Zunger parameters,  $6 \times 6 \times 4k$ -point grids, and 9.0 rgkmax are used. All APWs are converted into the linearized APWs for the calculations.
- [30]  $Q_{\text{ex}}$  behaves like  $\sim \alpha F_{i0}^4 F_{d0}^2 + \beta F_{i0}^3 F_{d0}^3 + \alpha F_{i0}^2 F_{d0}^4$  from  $((F_{i0} + F_{d0})^2)^3$  for relatively weak fields. This behavior may be further roughly simplified as  $\sim F_{i0}^3 F_{d0}^3$ .
- [31] T. Tamaya, A. Ishikawa, T. Ogawa, and K. Tanaka, *Phys. Rev. Lett.* **116**, 016601 (2016).
- [32] L. J. Boya, M. Kmiecik, and A. Bohm, *Phys. Rev. A* **37**, 3567 (1988).
- [33] U. Schwengelbeck and F. H. M. Faisal, *Phys. Rev. A* **50**, 632 (1994).
- [34] D. H. Gebremedhin and C. A. Weatherford, *Phys. Rev. E* **89**, 053319 (2014).
- [35] This is an expression of the long-wavelength sector of the (screened) Coulomb attraction incorporating a finite momentum width. In fact, how to treat the one-dimensional Coulomb potential has been a long standing problem due to the mathematical instability. To avoid the problem, soft core Coulomb potentials or nonsingular Coulomb potentials have been conventionally adopted [32–34] and the present study may be understood in a similar context.
- [36] B. Zaks, R. B. Liu, and M. S. Sherwin, *Nature (London)* **483**, 580 (2012).
- [37] F. Schlaepfer, M. Lucchini, S. A. Sato, M. Volkov, L. Kasmi, N. Hartmann, A. Rubio, L. Gallmann, and U. Keller, *Nat. Phys.* **14**, 560 (2018).